Numerical modelling of perforation impact damage of fibre metal laminates

* Jin Zhou[1], Zhongwei Guan[1] and Wesley Cantwell[2]

[1]School of Engineering, University of Liverpool, Liverpool L69 3GQ, UK
[2]Aerospace Research and Innovation Center (ARIC), Khalifa University of Science, Technology and Research (KUSTAR), Po.Box127788, Abu Dhabi, UAE.

*Jin Zhou: jinzhou@LIV.AC.UK

Abstract

Perforation damage of fibre metal laminates (FMLs) subjected to projectile impact was modelled using the finite element (FE) analysis. Here, FMLs studied covered stacking sequences of 2/1 and 3/2 FMLs, which were made with different aluminium alloys (6161-O, 6061-T6, 7075-O) and glass fibre reinforced polymer (GFRP) layers. A vectorized user-defined material subroutine (VUMAT) was developed to define Hashin's 3D rate-dependant damage criteria for the GFRP. The subroutine was implemented into the commercial finite element code ABAQUS/Explicit to simulate the deformation and failure of FMLs. The aluminium alloy layers were modelled as an isotropic elasto-plastic material by Johnson-Cook plasticity and the related damage criterion. The resin layer was simulated using cohesive elements, defined in terms of traction-separation. Good agreement was obtained between the simulations and the experimental results, in terms of the load–displacement traces, the deformation and failure modes.

Keywords: Impact, Fibre metal laminates, Hashin 3-D Criteria, Finite Element, Progressive Failure

1. Introduction

Fibre metal laminates (FMLs) are advanced composite structural materials that have been attracting interest from a number of researchers to investigate the impact resistance [Reyes and Cantwell (2000); Vogelesang and Vlot (2000)]. In recent years, a number of studies had been conducted to investigate the low and high velocity impact behaviour of fibre metal laminates. Caprino et al. [Caprino et al. (2004)] performed low-velocity impact tests on fibre metal laminates made of 2024-T3 sheets and S2-glass/epoxy prepreg layers. Various impact masses, velocities, and energies were applied in the tests to investigate the influence of these factors on the impact response. For comparison purposes, similar tests were also performed on monolithic 2024-T3 sheets with the equivalent thickness. Abdullah and Cantwell [Abdullah and Cantwell (2006)] studied the impact behaviour of a glass fibre reinforced polypropylene FMLs and the results showed that the FML offered an impressive resistance subject to low and high velocity impact. They found that FMLs absorb more energy during plastic deformation in the aluminium and composite layers. A low velocity impact tests on glass fibre-based FMLs has been conducted by Vlot and Fredell. The FMLs offer a superior impact to both an aluminium alloy and a carbon fibre reinforced composite. [Vlot and Fredell (1993)]. Vlot also conducted impact tests on an aluminium alloy and different types of FML and composites [Vlot (1996)]. There was a crack at the carbon and aramid fibres based FMLs and the energy absorption lower than that of a glass fibre reinforced FML. A inspection on the tested specimens showed that the FMLs exhibited a similar indentation in size to those plain aluminium alloy. Vlot et al. conducted impact tests on GLARE and plain aluminium and showed that the FML exhibited an initial cracking energy. They alos found that the impact damage resistance of these FMLs increased with increasing glass/epoxy content [Vlot et al (1999)].

A numbers of FE modeling have been developed to simulate the impact response of FMLs using numerical echniques. Guan et al investigated the impact response of fibre metal laminates based on a woven polypropylene (PP) fibre reinforced composite and an aluminium alloy at velocities up to 150 m/s. Both the predicted failure modes and displacement of the FMLs was good agree with the test data [Guan et al,(2009)]. Payeganeh et al. developed a number of FE models to investigate the resistance force traces, deflection, in-plane strains and stresses in of FMLs subjected to low velocity impact loading [Payeganeh et al. (2010)]. The results shown that the stacking sequence, the masses and velocities of the impactor were important parameters in determining the impact response of the FMLs. Lannucci et al studied the failure mode the impact load on FMLs. Modelling of composite damage subjected to impact within the intermediate strain rate regime may be generally categorized into four approaches [Lannucci (2006)], i.e. (1) failure criteria, (2) fracture mechanics, (3) plasticity or yield surface, and (4) damage mechanics. The Tsai-Wu failure criterion describes the failure surface in stress or strain space [Tsai and Wu (1971)]. However, it is a significant disadvantage to use stress-based failure criteria to model brittle materials as the scale effect in relation to the crack length in the same stress field cannot be modelled properly. Lee et al. [Lee et al. (2001)] investigated the penetration and perforation behaviour of a 6061-T6 aluminium plate and a C12K33 carbon fibre reinforced 6061-T6 aluminium metal-matrix composite plate subjected to projectile impact using an explicit finite element code, LS-DYNA3D. Perforation of the plate was found to occur under all of the studied impact conditions. The deformation behaviour of the plate and projectile as well as the projectile post-perforation velocity and the deceleration of the projectile were strongly dependent on the plate properties and impact velocity. Payeganeh et al. developed explicit FE models to investigate the contact force history, deflection, in-plane strains and stresses of 2024-O 2/1, 5/4 and 2024-T3 2/1, 5/4 FMLs subjected to low-velocity impact [Payeganeh et al. (2010)]. Failure shear strain and tension cut-off stresses were specified as failure criteria for aluminium layers. The failure of fibre laminate was simulated using Tsai–Wu failure criterion by specifying tensile cut-off stress based on the ultimate tensile stress of the fibre.

Although a few numerical modeling developed to simulate the response of composite using commercial software LS-DYNA and Abaqus. However, those such as ABAQUS only has a number of failure criteria for composite materials modeled using 2D elements, such as plane stress and continuum shell elements [Carla McGregor (2010)]. Further, none of these criteria consider strain-rate effects in composite materials, which is clearly important in dynamic studies. The 2D elements, with the existing failure criteria, are not capable of taking large through-the-thickness rate-dependent deformations into account. Therefore, it is necessary to develop a constitutive model with associated failure criteria suitable for simulating a composite material using 3D solid elements.

A limited numerical modeling were developed to investigate the structural response of composite using three-dimensional 3D solid elements. Recently, Thuc et al. developed a FE models which were validated using experimental data from tests on FMLs based on a 2024-O aluminium alloy and a woven glass–fibre/polypropylene composite. The rate-dependent failure criteria for a unidirectional composite were used, which were based on the modified Hashin's 3D failure criteria [Thuc et al. (2013]. The constitutive model and failure criteria were then implemented in ABAQUS/Explicit using the VUMAT subroutine. Based on the previous research [Thuc et al. (2013], A further parametric studies were carried out to investigate the influence of the properties of the aluminium alloy on the blast resistance of FMLs for aerospace applications. A vectorized user material subroutine (VUMAT) was employed to define Hashin's 3D rate-dependant damage constitutive model of the GFPP. [Thuc et al. (2014)] Sandwich panels based on three-dimensional woven S-glass/epoxy skins and a crosslinked PVC core were modelled using finite element techniques to investigate the effect of through-the-thickness stitching on the blast resistance of the

panels by [Guan et al. (2014)]. The finite element model accurately predicted the failure modes and deformed shapes of the sandwich panels over the range of impulsive loading conditions.

This paper presents numerical modeling of structural behavior of fibre metal laminates subjected to impact loading for aerospace applications. Here, Johnson–Cook strain hardening and damage criterion were employed to simulate the fialure of aluminiym layers. A vectorized user material subroutine (VUMAT) was employed to define Hashin's 3D damage criteria for the composite layer to model the corresponding deformation and failure mechanisms. Energy absorption of the fibre metal laminates plates made with different configurations of the liminates layers was also investigated. Modeling results were compared with the experimental results, in terms of load-displacement relationships, deformation and failure modes.

3 Finite element modeling

The two material layers in the FMLs, i.e. the composite and the aluminum alloy, exhibit very different mechanical behaviors. Therefore, different constitutive models were used to simulate the behavior of the metal and composite plies. The aluminium alloy layers were modelled as an isotropic elasto-plastic material by Johnson-Cook plasticity and the related damage criterion. ABAQUS/Explicit [Hibbitt et al. (2011)] was used to develop numerical simulations of the FMLs subjected to projectile impact. Numerical modeling was undertaken on the 6061-O, 6061-T6 and 7075-O FMLs outlined in Table 1.

Table 1 Johnson−Cook constants and static tensile strength for aluminium alloys

Aluminum type	A (MPa)	B (MPa)	n	C	D_1	D_2	D_3	D_4	Strength (MP)
Al 6061-T6	324	114	0.42	0.002	0.13	0.13	-1.5	0.011	332
Al 6061-O	360	105	0.73	0.083	0.013	0.025	-1.7	-0.4	310
Al 7075-O	535	658	0.71	0.024	-0.068	0.451	-0.95	0.036	551

3.1. Aluminium layers

The aluminium alloy was modelled as an elasto-plastic material included a rate-dependent behaviour. Temperature effects in the aluminium alloy were not taken into account. The Johnson−Cook material model was used in the form as below:

$$\sigma = [A + B(\bar{\varepsilon}_{pl})^n] \left[1 + C \ln \left(\frac{\dot{\bar{\varepsilon}}_{pl}}{\dot{\varepsilon}_0} \right) \right]$$

(1)

where $\bar{\varepsilon}_{pl}$ is the equivalent plastic strain; $\dot{\bar{\varepsilon}}_{pl}$ and $\dot{\varepsilon}_0$ are the equivalent plastic and reference strain rate and A, B, C and n are material parameters. Damage in the Johnson−Cook material model is predicted using the following cumulative damage law:

$$D = \sum \left(\frac{\Delta \bar{\varepsilon}_{pl}}{\bar{\varepsilon}_f^{pl}} \right)$$

(2)

in which

$$\bar{\varepsilon}_f^{pl} = [D_1 + D_2 \exp(D_3 \sigma^*)] \left[1 + D_4 \ln \left(\frac{\dot{\bar{\varepsilon}}_{pl}}{\dot{\varepsilon}_0} \right) \right]$$

(3)

3

where σ^* is the mean stress normalised by the equivalent stress and $\Delta\bar{\varepsilon}_{pl}$ is the increment of equivalent plastic strain during an increment in loading. D, is a function of the mean stress and the strain rate. The parameters D_1, D_2, D_3, and D_4 are constants. Failure is assumed to occur when D = 1. Hence the current failure strain, $\bar{\varepsilon}_f^{pl}$, and thus the accumulation of damage,. The constants in the Johnson−Cook model for the three alluminium alloys used in this study are given in Table 2. The Young's modulus, Poisson's ratio and density of the various aluminium alloys were taken as E = 73.5 GPa, ν = 0.3 and ρ = 2700 kg/m3, respectively.

3.2. Glass fibre reinforced composite layers

3.2.1. The 3D damage model for the composite material
A constitutive model and failure criteria suitable for simulating the solid geometry composite using 3D solid elements was employed to simulate the failure mechanism of glass fire layers. Failure criteria for laminated composites are available in ABAQUS, which can be applied for panel coordinate and continuum shell elements only. However, none of these existing criteria consider the third direction through-the-thickness and strain-rate effects in the composite material in a coordinate using 3D solid elements. In order to develop a constitutive model and failure criteria suitable for simulating the composite tube using 3D solid elements, a 3D rate-dependent failure criteria for a anisotropic composite is developed by modifying Hashin's 3D failure criteria [Hashin (1980), Thuc et.al (2012)], to include rate-dependent elastic moduli and strength properties. The failure criteria, with the related constitutive model, are implemented into ABAQUS/Explicit using a VUMAT subroutine provided by ABAQUS [ABAQUS Theory Manual. 6.11(2011)].

Given that a woven glass fibre composite layer is produced by placing fibres in a [0/90] pattern, the material behaviour within the plane of the laminate is similar in those two directions according to the material test data provided by the manufacturer. Therefore, the developed Hashin's 3D failure criteria [Thuc et.al (2013] be able to simulate overall response of a roll wrapped composite layer in a cylindrical coordinate. The failure functions may be expressed as follows:

Fibre tension: $\qquad (\sigma_{11} \geq 0): F_f^t = \left(\dfrac{\sigma_{11}}{X_{1t}}\right)^2 + \left(\dfrac{\sigma_{12}}{S_{12}}\right)^2 + \left(\dfrac{\sigma_{13}}{S_{13}}\right)^2, d_{ft} = 1$ $\qquad$ (4)

Fibre compression: $\qquad (\sigma_{11} < 0): F_f^c = \dfrac{|\sigma_{11}|}{X_{1t}}, d_{fc} = 1$ $\qquad$ (5)

Matrix tension: $\qquad (\sigma_{22} + \sigma_{33} \geq 0): F_m^t = \dfrac{(\sigma_{22} + \sigma_{33})^2}{X_{2t}^2} + \dfrac{\sigma_{23}^2 - \sigma_{22}\sigma_{33}}{X_{23}^2} + \dfrac{\sigma_{12}^2 + \sigma_{13}^2}{X_{12}^2}, d_{mt} = 1$ $\qquad$ (6)

Matrix compression: $(\sigma_{22} + \sigma_{33} \geq 0):$

$$F_m^c = \left[\left(\frac{X_{2c}}{2S_{23}}\right)^2 - 1\right]\frac{(\sigma_{22} + \sigma_{33})}{X_{2c}^2} + \frac{(\sigma_{22} + \sigma_{33})^2}{4S_{23}^2} + \frac{\sigma_{23}^2 - \sigma_{22}\sigma_{33}}{X_{23}^2} + \frac{\sigma_{12}^2 + \sigma_{13}^2}{X_{12}^2}, d_{mc} = 1 \qquad (7)$$

where X_{1t}, X_{1c}, X_{2t}, X_{2c}, S_{12}, S_{13} and S_{23} are the various strength components and d_{ft}, d_{fc}, d_{mt} and d_{mc} are the damage variables associated with the four failure modes.

4

The response of the material after damage initiation (which describes the rate of degradation of the material stiffness once the initiation criterion is satisfied) is defined by the following equation:

$$\sigma = C(d) \cdot \varepsilon \ , \ \sigma_{ij} = C_{ij} \cdot \varepsilon_{ij} \tag{8}$$

$$\begin{bmatrix} \sigma_{11} \\ \sigma_{22} \\ \sigma_{33} \\ \sigma_{12} \\ \sigma_{23} \\ \sigma_{13} \end{bmatrix} = \begin{bmatrix} C_{11}^0 & C_{12}^0 & C_{13}^0 & & & \\ C_{12}^0 & C_{22}^0 & C_{23}^0 & & & \\ C_{13}^0 & C_{23}^0 & C_{33}^0 & & & \\ & & & C_{44}^0 & & \\ & & & & C_{55}^0 & \\ & & & & & C_{66}^0 \end{bmatrix} \begin{bmatrix} \varepsilon_{11} \\ \varepsilon_{22} \\ \varepsilon_{33} \\ \varepsilon_{12} \\ \varepsilon_{23} \\ \varepsilon_{13} \end{bmatrix} \tag{9}$$

where C_{ij} is a 6 x6 symmetric damaged matrix, whose non-zero terms can be written as:

$$C_{11} = (1 - d_f)E_1(1 - v_{23}v_{32})\Gamma$$

$$C_{22} = (1 - d_f)(1 - d_m)E_2(1 - v_{13}v_{31})\Gamma$$

$$C_{33} = (1 - d_f)(1 - d_m)E_3(1 - v_{12}v_{21})\Gamma$$

$$C_{12} = (1 - d_f)(1 - d_m)E_1(v_{21} - v_{31}v_{23})\Gamma$$

$$C_{23} = (1 - d_f)(1 - d_m)E_2(v_{32} - v_{12}v_{31})\Gamma \tag{10}$$

$$C_{31} = (1 - d_f)(1 - d_m)E_1(v_{31} - v_{21}v_{32})\Gamma$$

$$C_{44} = (1 - d_f)(1 - s_{mt}d_{mt})E_1(1 - s_{mc}d_{mc})G_{12}$$

$$C_{55} = (1 - d_f)(1 - s_{mt}d_{mt})E_1(1 - s_{mc}d_{mc})G_{23}$$

$$C_{66} = (1 - d_f)(1 - s_{mt}d_{mt})E_1(1 - s_{mc}d_{mc})G_{13}$$

where the global fibre and matrix damage variables as well as the constant Γ are also defined as:

$$d_f = 1 - (1 - d_{ft})(1 - d_{fc})$$

$$d_m = 1 - (1 - d_{mt})(1 - d_{mc}) \tag{11}$$

$$\Gamma = 1/(1 - v_{12}v_{21} - v_{23}v_{32} - v_{13}v_{31} - 2v_{21}v_{32}v_{13})$$

where E_i is the Young's modulus in the i direction, G_{ij} is the shear modulus in the i–j plane and v_{ij} is the Poisson's ratio for transverse strain in the j-direction, when the stress is applied in the i-direction. The Young's moduli, shear's moduli, Poisson's ratios and strengths of the CFPP are given in Table 2 and 3. The factors s_{mt} and s_{mc} in the definitions of the shear moduli are introduced to control the reduction in shear stiffness caused by tensile and compressive failure in the matrix respectively. The following values are recommended in [ABAQUS Theory Manual (2011)]: $s_{mt} = 0.9$ and $s_{mc} = 0.5$.

Table 2. Properties data for the GFRP composite

E_1 (MPa)	E_2 (MPa)	E_3 (MPa)	G_{12} (MPa)	G_{13} (MPa)	G_{23} (MPa)	v_{12} (MPa)	v_{13} (MPa)	v_{23} (MPa)	ρ (kg/m^3)
13	13	2.4	1.72	1.72	1.72	0.1	0.3	0.3	1800

Table 3. Damage initiation data for the GFRP composite

X_{1T} (MPa)	X_{1C} (MPa)	X_{2T} (MPa)	X_{2C} (MPa)	S_{12} (MPa)	S_{13} (MPa)	S_{23} (MPa)
320	240	320	240	140	140	140

2.2.2. Strain-rate effects in the mechanical properties

The effects of strain-rate on the mechanical properties of a composite material are typically modelled using strain-rate dependent functions for both the elastic modulus and the strength. Yen [Yen (2012)] developed logarithmic functions to account for strain-rate effects in a composite material as follows:

$$\{S_{RT}\} = \{S_0\}\left(1 + C_1 In \frac{\dot{\bar{\varepsilon}}}{\dot{\bar{\varepsilon}}_0}\right)$$

$$\{E_{RT}\} = \{E_0\}\left(1 + C_2 In \frac{\dot{\bar{\varepsilon}}}{\dot{\bar{\varepsilon}}_0}\right) \quad (12)$$

Where

$$\{\dot{\bar{\varepsilon}}\} = \left\{|\dot{\varepsilon}_1| \quad |\dot{\varepsilon}_2| \quad |\dot{\varepsilon}_1| \quad |\dot{\varepsilon}_2| \quad |\dot{\varepsilon}_{12}| \quad |\dot{\varepsilon}_{13}| \quad |\dot{\varepsilon}_{23}|\right\}^T$$

$$\{S_{RT}\} = \{X_{1t} \quad X_{2t} \quad X_{1c} \quad X_{2c} \quad S_{12} \quad S_{13} \quad S_{23}\}^T \quad (13)$$

$$\{E_{RT}\} = \{E_1 \quad E_2 \quad E_3 \quad G_{12} \quad G_{13} \quad G_{23}\}^T$$

and the subscript RT refers to the rate-adjusted values, the subscript 0 refers to the static value, $\dot{\bar{\varepsilon}} = 1^{-1}$ is the reference strain-rate, $\dot{\bar{\varepsilon}}$ is the effective strain-rate, C_1 and C_2 are the strain-rate constants, respectively.

2.3 Cohesive elements and material properties

The resin layer at the interface between 0° lateral axis and oriented at 90° across its diameter plies was modelled using cohesive elements available in ABAQUS [ABAQUS Users Manual (2011)]. The elastic response was defined in terms of a traction-separation law with uncoupled behaviour between the normal and shear components. The default choice of the constitutive thickness for modelling the response, in terms of traction versus separation, is 1.0, regardless of the actual thickness of the cohesive layer. Thus, the diagonal terms in the elasticity matrix and density should be calculated using the true thickness of the cohesive layer as follows:

$$K_{nn} = \frac{E_n}{t_c}, \quad K_{ss} = \frac{E_s}{t_c}, \quad K_{tt} = \frac{E_t}{t_c}, \quad \rho = \rho_c t_c \quad (14)$$

6

The quadratic nominal stress and energy criterion were used to model damage initiation and damage evolution, respectively. Damage initiated when a quadratic interaction function, involving the nominal stress ratios, reached unity. Damage evolution was defined based on the energy conjunction with a linear softening law. The mechanical properties of the cohesive elements were obtained from [Karagiozova et al. (2010)].

3 Implementation of the material model in ABAQUS/Explicit

The user defined VUMAT subroutine was developed to implement the material model and failure criteria described in the previous sections in ABAQUS/Explicit. During each time step of computation, this subroutine is compiled and enables ABAQUS/ Explicit to obtain the required information regarding the state of the material and the material mechanical response at each integration point of each element. The Hashin's 3D failure criteria outlined in equations (4-7) are calculated, and the elastic modulus and strength values are adjusted for strain-rate effects using equations (11) base on these stresses computed within the VUMAT subroutine using the given strains and the material stiffness coefficients. The element status, which determined by the failure criteria, is then changed from 1 to 0 when an element fails. Accompanying the change of element status, the stresses at that material point are reduced to zero and it no longer contributes to the model stiffness. The element is removed from the mesh when all of the material status points of an element have been reduced to zero.

The fibre metal laminates consisted of the aluminum, the composite and the cohesive layers as three separate parts. The aluminum and composite layers for CFRP tubes were meshed using C3D8R elements, which are eight-noded, linear hexahedral elements with reduced integration and hourglass control. The mesh generation and boundary conditions shown in Figure 1. The interfaces between the composite layers were created using eight-node 3D cohesive elements (COH3D8). The plate size is 75×75 (in mm). The initial velocity applied to the projectile, with an only degree of freedom in the vertical direction. The plate edges are fully fixed. Given that the panels were symmetric in nature, a quart of each panel was modeled with the appropriate boundary conditions applied along the planes of symmetry. A condition of general contact interaction was defined between the two neighboring layers of composites. Surface-based tie constraints were imposed between the composite layer and the cohesive layer to model adhesion between the adjacent layers. The contact interaction property for interaction between the aluminum and composite layer was also defined.
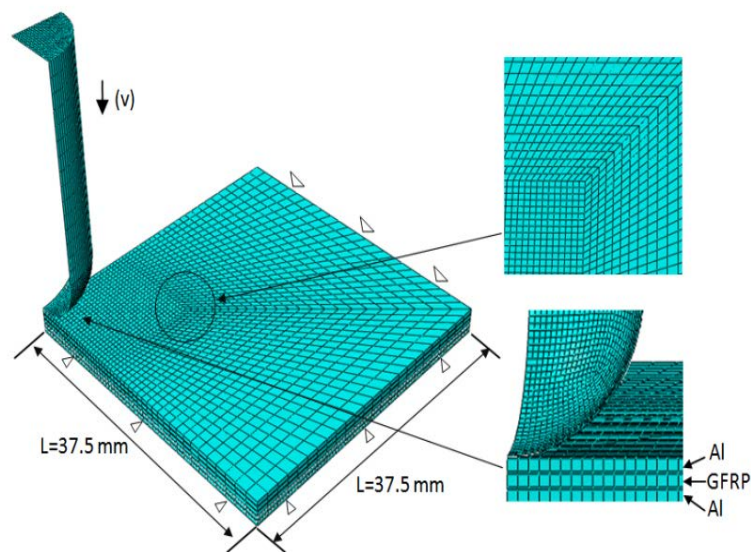

Figure 1 The geometry, mesh, boundary and loading conditions of the model for FMLs.

4 Results and Discussion

The developed finite element models have been simulated to predict the structural behaviour of fibre metal laminates subject to perforation loading. Modeling results were compared with the experimental results, in terms of load-displacement relationships, energy absorption, deformation and failure modes. The perforation loading on individual layers has been modeling firstly to validation the FE modeling. The perforation prediction on FMLs has been compared with the experimental data.

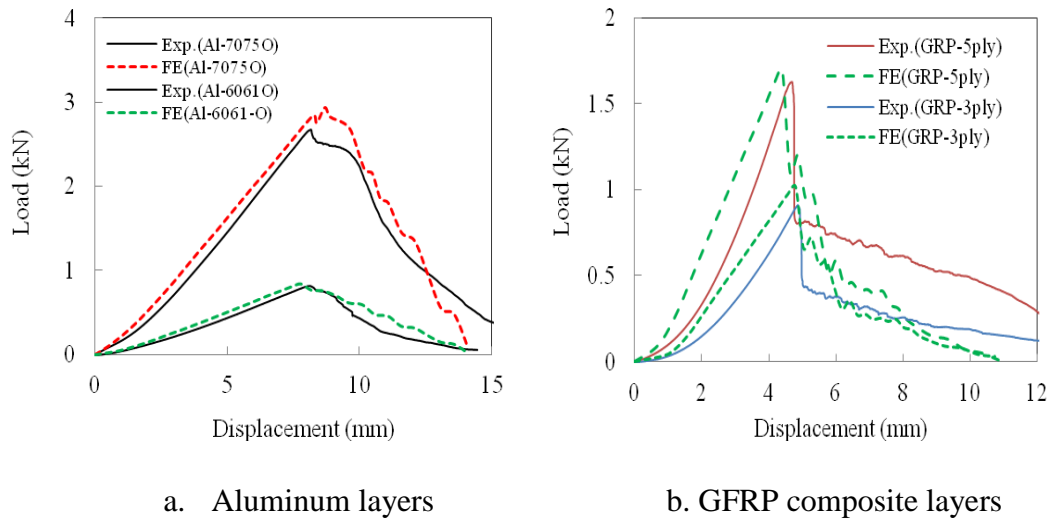a. Aluminum layers   b. GFRP composite layers

Figure. 2 Comparison of load-displacement traces of perforation tests for individual layers on aluminum and GFRP

Figures 2a show the comparison between the experimental and the numerical load-displacement traces for the individual layers of the 6061-o and 7075-O aluminums. The peak loads from the numerical predictions and the experimental tests for these layers were 750 and 3105 N, respectively. The former are only 3.1% and 9.2% higher than the latter, respectively. Also the predicted initial stiffness and the displacement at the peak load for the two aluminum were shown a good agreement with the corresponding experimental results. The predicted perforation energies were 5.8 and 20.8 J respectively, which are only 5.8% higher and 6.4% higher than the corresponding experimental results. Figures 2b present the comparison between the experimental and the numerical load-displacement traces for the 0.5 mm 3-ply and 1 mm 5-ply composite layers respectively subjected to a low velocity impact. The load-displacement traces shows that the stiffness is lower at beginning and the traced start liner up after the displacement of 1 mm. The peak loads from the numerical predictions and the experimental tests for these layers were 1015 and 1692 N, respectively. The former are only 4.1% and 7.2% higher than the latter, respectively. Also the predicted initial stiffness and the displacement at the peak load for the two GRP skins were in reasonably good agreement with the corresponding experimental results. The predicted perforation energies were 3.35 and 5.51 J respectively, which are only 5.8% higher and 6.4% higher than the corresponding experimental results. The fibre metal laminate was simulated using the validated individual layers.

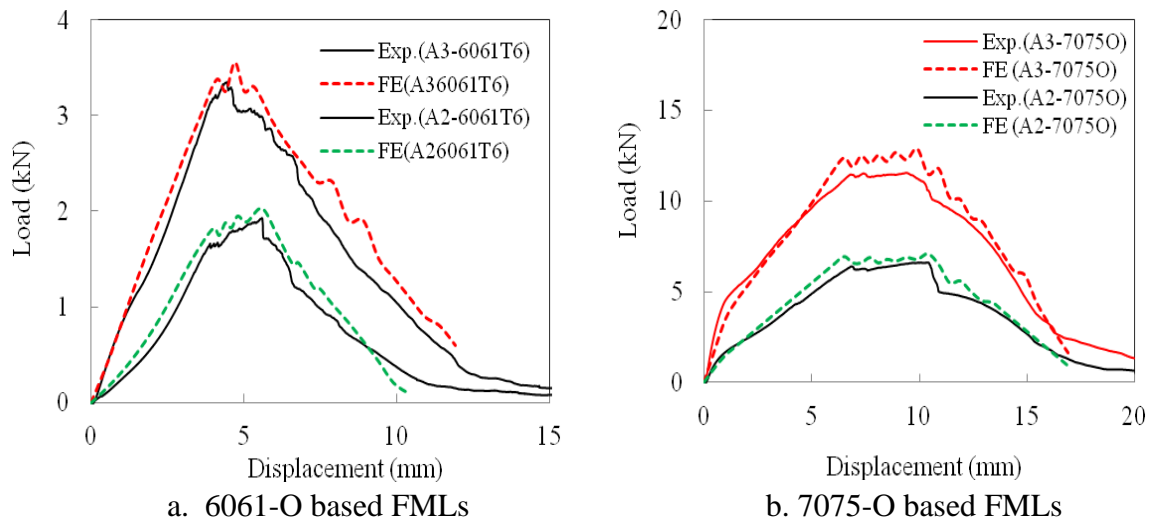|	
a. 6061-O based FMLs	b. 7075-O based FMLs

Figure. 3 Comparison of load-displacement traces of 2/1 and 3/2 fibre metal laminates between FE and experimental tests.

The finite element models using the constitutive models and failure criteria presented in the figure 2 were developed to simulate the critical perforation impact tests of various fibre metal laminates. Figures 3a and 3b show the simulated and the related experimental load-displacement traces of 2/1 and 3/2 FMLs plates made with 3-ply and 5-ply composite layers respectively subjected to low velocity impact. Figure 3a shows the 0.5 mm thick 6061-O aluminum and 3-ply GFRP based FMLs. The load-displacement traces show a linear up stiffness until the fist peak load. The predicted peak loads for the 6061-O based 2/1 and 3/2 FMLs plates were 203 and 355 Newtons, respectively, which are 2.4% and 6.0% higher than the experimental results respectively. The predicted initial stiffness and the displacement at the peak load for the targets were in good agreement with the corresponding experimental results. The predicted perforation energies were 11.09 and 23.65 Joules, respectively. In comparison with the experimental results they were slightly higher, respectively.

Figure 3b shows the 1 mm thick 7075-O aluminum and 5-ply GFRP based FMLs. The load-displacement traces show a linear up stiffness up to the displacement of 1 mm. The stiffness reduced and shows a lower liner stiffness before up to first peak load. The reduced stiffness maybe caused by the delamination between aluminum and composite layer which cased the stiffness reduced. The predicted peak loads for the 7075-O based 2/1 and 3/2 FMLs plates were 7100 and 12900 Newtons, respectively, which are 5.4% and 8.1% higher than the experimental results respectively. The predicted initial stiffness and the displacement at the peak load for the targets were in reasonably agreement with the corresponding experimental results. The predicted perforation energies were 74.4 and 132.5 Joules, respectively. In comparison with the experimental results the results still slightly higher.

	Exp.	FE

2/1

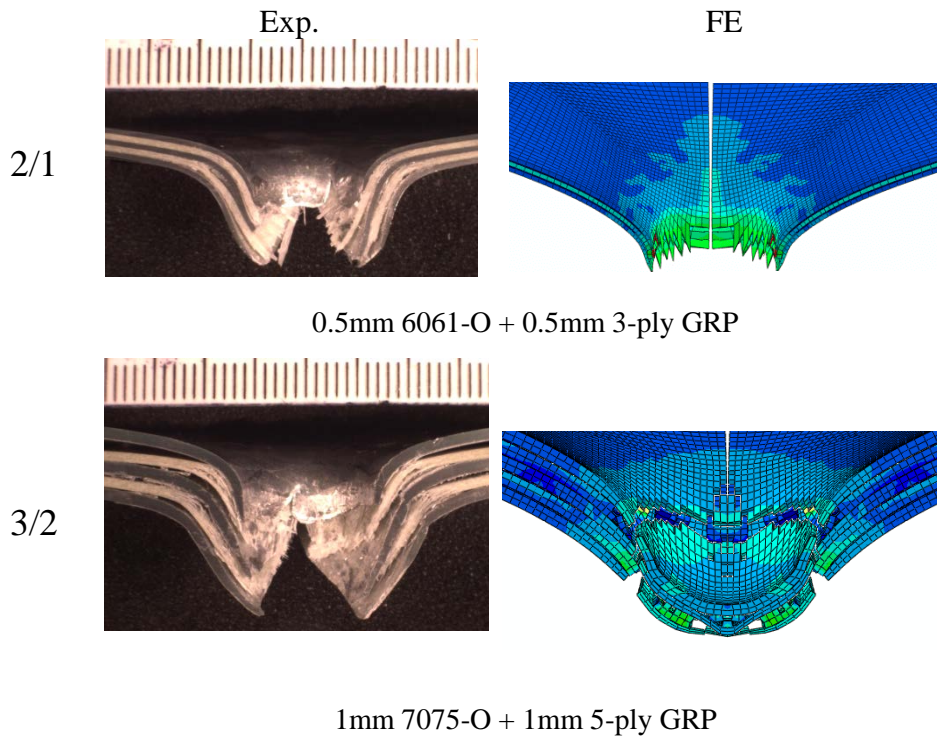0.5mm 6061-O + 0.5mm 3-ply GRP

3/2

1mm 7075-O + 1mm 5-ply GRP

Figure 5 Comparison of the simulated and experimental failure modes of 3/2 FMLs plates made with 3-ply and 5-ply composite

Figures 5 show the comparison of the simulated and experimental failure modes of 3/2 FMLs plates made with 3-ply and 5-ply composite subjected to an on-set perforation impact. The basic features of the experimental failure modes for all the FMLs plates were well simulated, in terms of the cross cracks at the rear face and the local deformation mode at the target centre. Since the difference between the FMLs plates was thickness of aluminum and the number of composite plies in the composite layer, the experimental failure modes for these two FMLs plates were quite similar. The FE simulate the delamination of resin between composite and aluminum.
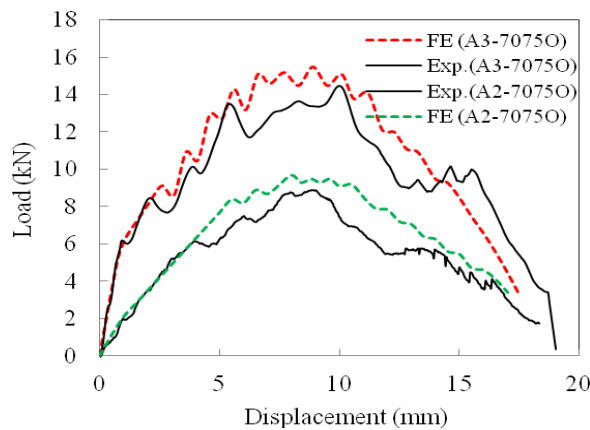

Figure. 6 Comparison of load-displacement traces of impact tests on 2/1 and 3/2 7075-O based fibre metal laminates between FE and experimental tests.

Finite element models of other types of FMLs plates subjected to a low velocity impact were also developed include the strain rate effects to broaden the validation. Figures 6 show the numerical simulations of the experimental load-displacement traces for the 3/2 FMLs plates made with 5-ply composite cores respectively subjected to an on-set perforation impact. Very good correlation was obtained between the experimental results and the numerical simulations, in terms of the overall

initial stiffness, the peak load and the perforation process. The predicted peak loads for these two FMLs plates were 970 and 1551 N, respectively, which are only 5.4 % and 5.8 % higher in comparison with the experimental results, respectively. The predicted initial stiffness and the predicted displacement at the peak load were also shown reasonably agreement with the corresponding experimental results. The predicted perforation energies for these two plates were 103.4 and 175.5 J, respectively. Compared to the experimental results, the FE were reasonable higher.
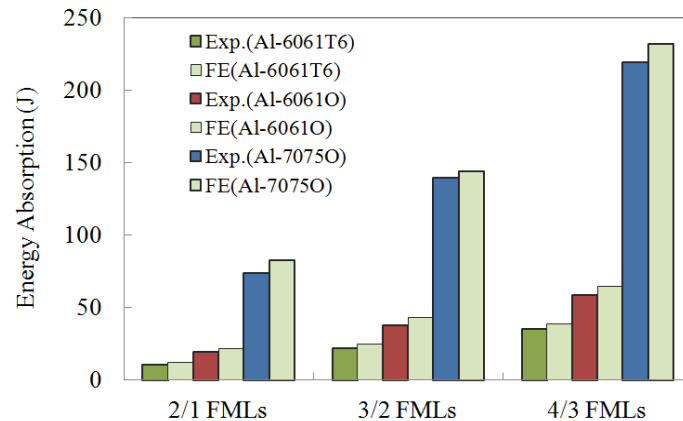

Figure. 7 Comparison of energy absorption of 2/1, 3/2 and 4/3 fibre metal laminates between FE and experimental tests.

Figures 7 show the comparison between the the perforation energy and the corresponding test results in a chart form. Clearly, very good correlation was obtained. The green bar show the FE prediction of the modeling and all the FE results are slight higher than the experimental data as the load-displacement traces shown in early figure. The possible reason may caused by the contact parameters used for the contact between projectile and FMLs, the strain rate of the modeling, elements control of the modeling. In further studies, more points can to be predicted by using validated numerical models in order to draw out the reliable relationship, In fact, the finite element models developed are well validated based on the reasonably good prediction compare to the test results.

Conclusions

Finite element models have been developed to simulate the structural behaviour of fibre metal laminates with various stacking sequences and three different aluminium alloys subjected to impact loading. Hashin's 3D failure criteria, incorporating strain-rate effects in the GFPP is implemented into ABAQUS/Explicit using a vectorized user-defined material subroutine (VUMAT). Very good correlation has been obtained between the numerical simulations and the experimental results, in terms of load-displacement traces, peak load and perforation energy. A reasonable agreemetn bas been shown in deformation mode and failure mode.

The validated finite element models, which cover the configurations of 2/1, 3/2 and 4/3 laminates made with different layers included 3-ply and 5-ply composite and various thinckness of aluminiums are ready to be used for further parametric studies of FMLs subjected to different loading conditions. The evidence suggests that the impact resistance and energy absorption increased with the increasing of laminates thickness and area density. Both the peak load and erergy absorption of 6061-T6 overperform than the 6061-O based fibre metal laminates, however the specifii erergy absorption of later slight higher than former. It also a suggests that the 7075-O alloy offers the best impact resistance and energy absorptions.

References

ABAQUS/Explicit, Users Manual, Version 6.11（2011）, Hibbitt, Karlsson & Sorensen, Inc.

ABAQUS, Theory Manual. Version 6.11（2011）. Pawtucket: Hibbitt, Karlsson & Sorensen, Inc.

Abdullah MR, Cantwell WJ (2006) The impact resistance of polypropylene-based fibre metal laminates. *Compos Sci Technol*;66:1682–93.

Caprino G, Spataro G, Del LS (2004). Low-velocity impact behaviour of fibreglassaluminium laminates. *Compos Part A,* 35:605–16.

Deshpande V.S.. and Fleck N.A.（2001）"Multi-axial yield behavior of polymer foams", *Acta mater*., Vol. 49, 1859–1866.

Fan J., Guan Z.W. and Cantwell W.J.（2011）Numerical modelling of perforation failure in fibre metal laminates subjected to low velocity impact loading. *Composite Structures*, Vol. 93, pp2430–2436.

ABAQUS/Explicit, *Users Manual, Version 6.11（2009）*, Hibbitt, Karlsson & Sorensen, Inc.

ABAQUS, *Theory Manual. Version 6.11（2012）*. Pawtucket: Hibbitt, Karlsson & Sorensen, Inc.

Guan ZW, Cantwell WJ, Abdullah R. Numerical modeling of the impact response of fibre-metal laminates. *Polym Compos* 2009;30:603–11.

Guan Z.W, Aktas A., Potluri P., Cantwell W.J., Langdon G., Nurick G.N. (2014), The blast resistance of stitched sandwich panels, *International Journal of Impact Engineering* 65, 137e145

Hashin Z. Failure criteria for unidirectional fiber composites(1980), *J Appl Mech.* 47,329–34.

Karagiozova D, Langdon GS, Nurick GN, Yuen SCK (2010). Simulation of the response of fibre–metal laminates to localised blast loading. *Int J Impact Eng;37*(6):766–82.

Lee W S, Lai C H, Chiou S T (2001). Numerical study on perforation behaviour of 6061-T6 aluminium matrix composite. *J Mater Process Technol*, , 117: 125–131

Payeganeh GH, Ghasemi FA, Malekzadeh K. (2010) Dynamic response of fibre-metal laminates (FMLs) subjected to low-velocity impact. *Thin-Walled Struc*;48:62–70

Reyes G, Cantwell WJ (2000). The mechanical properties of fibre-metal laminates based on glass fibre reinforced polypropylene. *Compos Sci Technol*;60:1085–94.

Lannucci L (2006). Progressive failure modelling of woven carbon composite under impact. *Int J Impact Eng,* , 32: 1013–1043

Tsai S W, Wu E (1971). A general theory of strength for anisotropic materials. J Compos Mater, , 5: 58–80

Vlot A, Fredell RS (1993). Impact damage resistance and damage tolerance of fibre metal laminates. *In: Proceedings of the 9th international conference on composite materials Spain*, vol.6;. p. 51–8.

Vlot A (1996). Impact loading on fibre metal laminates. Int J Impact Eng;18:291–307.

Vlot A, Vogelesang LB, Vries T (1999). Towards application of fibre metal laminates in large aircraft. *Aircraft Eng Aerospace Technol;*71:558–70.

Vogelesang LB (2000), Vlot A. Development of fibre metal laminates for advanced aerospace structures. *J Mater Process Technol*;103:1–5.

Vo TP, Guan ZW, Cantwell WJ, Schleyer GK,(2012). Low-impulse blast behaviour of fibre–metal laminates. *Compos Structures,* 94(3),:954–65.

Vo TP, Guan ZW, Cantwell WJ, Schleyer GK(2013). Modelling of the low-impulse blast behaviour of fibre–metal laminates based on different aluminium alloys, *Composites: Part B* 44, 141–151